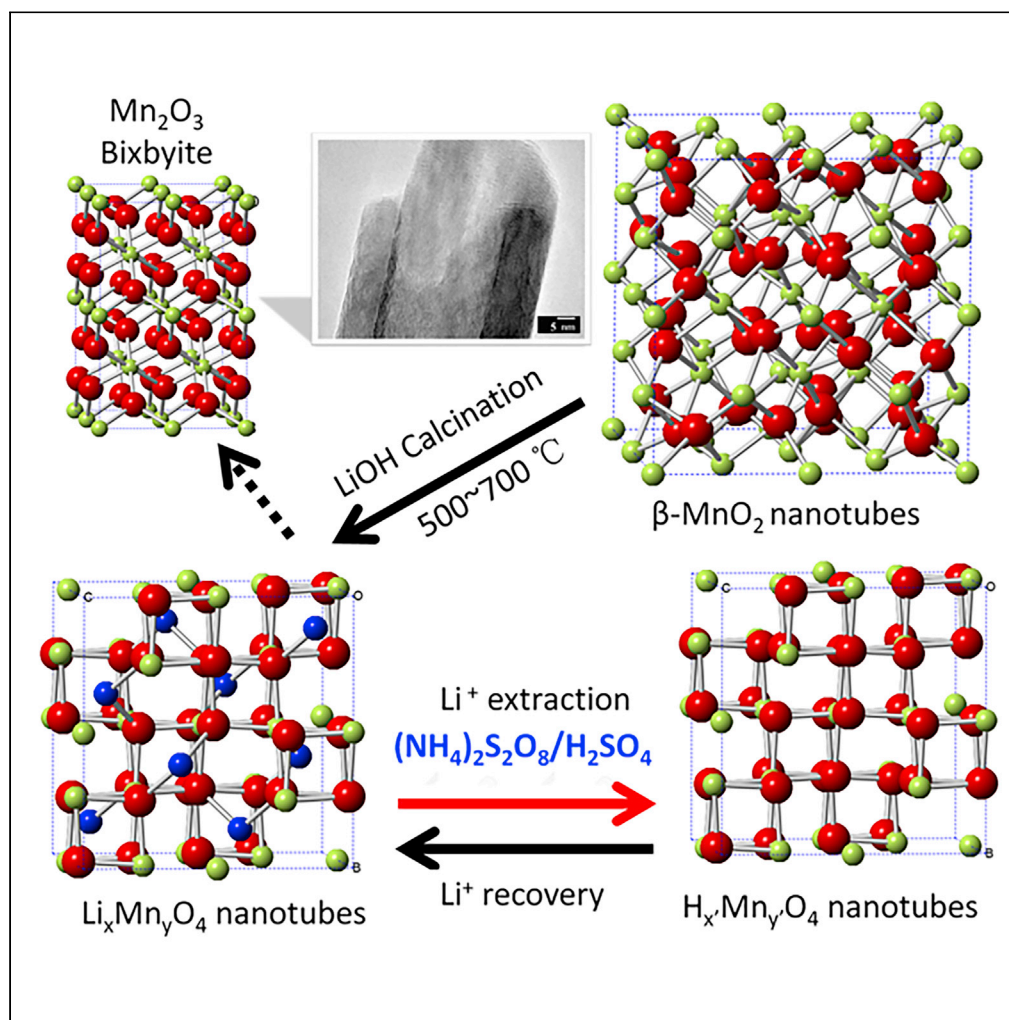


Article

Extraction of Lithium from Single-Crystalline Lithium Manganese Oxide Nanotubes Using Ammonium Peroxodisulfate



Kaiyuan Shi,
Mingwu Luo, Jie
Ying, Shunying
Zhen, Zhenyu
Xing, Ri Chen

shiky7@mail.sysu.edu.cn (K.S.)
xingzhenyu@m.scnu.edu.cn
(Z.X.)

HIGHLIGHTS

Single-crystalline
 $\text{Li}_{1.1}\text{Mn}_{1.9}\text{O}_4$ nanotubes
were developed for
lithium extraction

The sorbent showed Li/
Mn ratio depletion over
adsorption/desorption
processes

Acid-free extraction
minimized the structural
change and Mn reduction

Acid-free extraction
improved the chemical
stability and reusability of
the sorbent

Article

Extraction of Lithium from Single-Crystalline Lithium Manganese Oxide Nanotubes Using Ammonium Peroxodisulfate

Kaiyuan Shi,^{1,6,*} Mingwu Luo,¹ Jie Ying,² Shunying Zhen,³ Zhenyu Xing,^{3,*} and Ri Chen^{4,5}

SUMMARY

In this work, a spinel single-crystalline $\text{Li}_{1.1}\text{Mn}_{1.9}\text{O}_4$ has been successfully synthesized using $\beta\text{-MnO}_2$ nanotubes as the self-sacrifice template. The tubular morphology was retained through solid-state reactions, attributed to a minimal structural reorganization from tetragonal $\beta\text{-MnO}_2$ to spinel $\text{Li}_{1.1}\text{Mn}_{1.9}\text{O}_4$. The materials were investigated as sorbents for lithium recovery from LiCl solutions, recycled using H_2SO_4 and $(\text{NH}_4)_2\text{S}_2\text{O}_8$. $\text{Li}_{1.1}\text{Mn}_{1.9}\text{O}_4$ nanotubes exhibited favorable lithium extraction behavior due to tubular nanostructure, single-crystalline nature, and high crystallinity. $(\text{NH}_4)_2\text{S}_2\text{O}_8$ eluent ensures the structural stability of $\text{Li}_{1.1}\text{Mn}_{1.9}\text{O}_4$ nanotube, registering a Li^+ adsorption capacity of 39.21 mg g^{-1} ($\sim 89.73\%$ of the theoretical capacity) with only 0.08% manganese dissolution after eight adsorption/desorption cycles, compared to that of 1.21% for H_2SO_4 . It reveals the degradation of sorbent involves with the volume change, Mn reduction, and Li/Mn ratio depletion. New strategies, based on nanotube adsorbent and $(\text{NH}_4)_2\text{S}_2\text{O}_8$ eluent, can extract lithium ions at satisfactorily high degrees while effectively minimizing manganese dissolution.

INTRODUCTION

The demand for lithium production worldwide has significantly increased in recent years due to the growth of the rechargeable lithium-ion battery market (Li et al., 2018). The sources of lithium are mainly in forms of water resources and ore bodies, such as spodumene, lepidolite, and petalite ores. The grown interest in lithium extraction derived from water resources is attributed to its low cost, natural abundance, and environmental friendliness (Battistel et al., 2020). Great efforts have been devoted to selective recovery of Li^+ from water resources, including precipitation (Biswal et al., 2018), evaporative crystallization (Ooi et al., 2017), solvent extraction (Zhang et al., 2020), electrochemical adsorption (Battistel et al., 2020; Du et al., 2016), and ion exchange adsorption (Lin et al., 2019; Wang et al., 2020). The precipitation and evaporative crystallization are limited for processing high concentrated Li^+ solutions, which requires a pre-concentration process that entails tedious treatment and large energy consumption. Although the solvent extraction indicates high selectivity of lithium, the use of organic solvents generates significant environmental concerns. Electrochemical adsorption, based on the redox reactions of electrodes, has attracted increasing attention (Pasta et al., 2012; Trócoli et al., 2017). In this technique, the materials are regenerated using an external power source, which avoided the use of chemicals for adsorbent regeneration; however, the method exhibits irreversible electrochemical reactions and limited lithium productions due to low energy efficiency (Pasta et al., 2012).

Lithium-ion sieve technology represents a cost-effective green method, based on functional adsorbents capturing of lithium ions from the brines (Paranthaman et al., 2017; Tang et al., 2020; Xu et al., 2016). Among various materials, spinel-type lithium manganese oxides $\text{Li}_x(\text{Mn}^{\text{III}}\text{Mn}^{\text{IV}})\text{O}_4$ or LMOs attract more attention from academic researchers and, more recently, from the industry due to feasible production, excellent selectivity, and high lithium uptake capacity (Liu et al., 2019; Safari et al., 2020). A lithium-ion sieve is derived from the extraction of Li^+ from spinel-type LMOs (Luo et al., 2016). In general, mild acids are employed for an ion exchange between Li^+ and H^+ , yielded to a hydrogen manganese oxide (HMO) (Choi et al., 2020; Hong et al., 2018; Zhang et al., 2019). However, the promise of LMOs has been hampered by its low chemical stability in the acidic environment (Wang et al., 2020; Wei et al., 2020). It is known that the Mn^{III} in the LMOs can undergo a disproportionation transaction and turn into Mn^{II} and Mn^{IV} upon delithiation (Hayashi

¹School of Materials Science and Engineering, Sun Yat-Sen University, Guangzhou, Guangdong 510275, China

²School of Chemical Engineering and Technology, Sun Yat-Sen University, Zhuhai, Guangdong 519082, China

³School of Chemistry, South China Normal University, Guangzhou, Guangdong 510006, China

⁴School of Electromechanical Engineering, Guangdong Polytechnic Normal University, Guangzhou, Guangdong 510635, China

⁵School of Electromechanical Engineering, Guangdong University of Technology, Guangzhou, Guangdong 510006, China

⁶Lead Contact

*Correspondence: shiky7@mail.sysu.edu.cn (K.S.), xingzhenyu@m.scnu.edu.cn (Z.X.)

<https://doi.org/10.1016/j.isci.2020.101768>



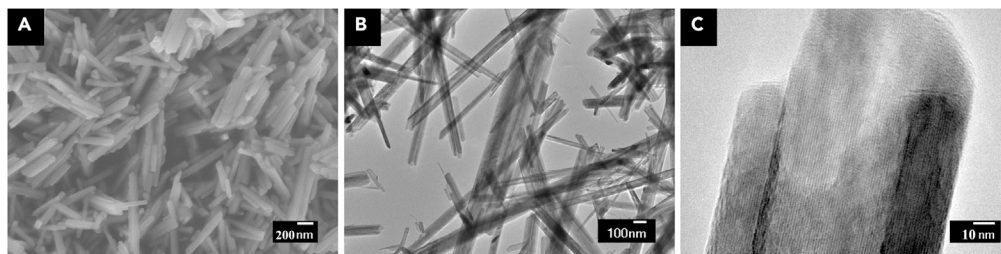


Figure 1. Morphology of LMO Nanotubes

(A–C) (A) SEM image and (B and C) TEM images of LMO nanotubes at different magnifications.

et al., 2016). The collapse of the spinal structure, triggered by the Mn^{II}/Mn^{IV} dissolution, degrades the performance and reusability of the sorbent. Therefore, the acidic treatment poses a persistent challenge for LMO implementations of lithium exploitations.

The interest in applications of nanostructured sorbents for lithium extraction is attributed to its high surface area and high adsorption capacity (Du et al., 2016; Kamran et al., 2019; Luo et al., 2016). However, relatively poor stability has been achieved. The adsorption performance strongly depends on the morphology, porosity, and crystalline structure of the material (Xu et al., 2016). One-dimensional nanomaterial with enlarged surface area and accessible extraction-desorption sites is promising for lithium recovery (Moazeni et al., 2015). The nanostructured network facilitates favorable ion transportation, thus allowing high Li^+ uptake capacity and fast recovery kinetics (Tang et al., 2013; Wu and Zhao, 2011). It has been demonstrated that single-crystalline material boosts efficient and reversible lithiation/delithiation processes due to its well-defined geometry, short Li^+ ions diffusion length, and perfect crystallization (Ding et al., 2011). In this study, we synthesized a single-crystalline LMO nanotube, with a composition of $Li_{1.1}Mn_{1.9}O_4$, for the selective recovery of Li^+ from LiCl solutions and simulated brines. The reusability and adsorption performance of LMO nanotubes was ensured using ammonium persulfate ($(NH_4)_2S_2O_8$) as the eluent.

RESULTS

Figure 1A shows a typical Scanning Electron Microscope (SEM) image of LMO nanotubes prepared by a template-engaged synthesis using β - MnO_2 nanotubes as the precursor. The LMO nanotubes exhibited a length and a width in a range of 0.5–2 μm and 70–200 nm, respectively. The interior hollow structure of LMO nanotubes was observed by Transmission electron microscope (TEM) (Figures 1B and 1C). The formation of β - MnO_2 templates (Figures S1A and S1B, Supplemental Information), based on the hydrothermal process, encompasses through a nucleation-dissolution-anisotropic growth-recrystallization mechanism. The growth of β - MnO_2 tubular structures involves the dissolution and recrystallization of γ - $MnOOH$ as intermediates. The tips of β - MnO_2 templates exhibit a sharp boundary as the material undergoes a phase transition from the intermediates to β - MnO_2 , leading to a tubular nanostructure (Figures S1C and S1D, Supplemental Information). This morphology is effectively maintained during the subsequent solid-state reaction (Figure 1B). The aspect ratio of nanotubes is increased, indicated that the tubes slightly swell in the direction perpendicular to the tube axis through the template-engaged transformation process. High-resolution TEM results reveal a single-crystalline structure of LMO nanotube, with an inner and outer diameter of 48 and 70 nm, respectively (Figure 1C). The composition and crystal structure of obtained LMO nanotubes were analyzed by Inductively Coupled Plasma-Optical Emission Spectroscopy (ICP-OES) and X-ray Diffraction (XRD) characterizations. The nanotubes demonstrated a well-crystallized cubic spinel structure with the $Fd3m$ symmetry (Figure S2, Supplemental Information). The lattice constant is calculated to be 8.239 \AA , which is slightly smaller than that of the literature value (8.248 \AA , JCPDS No. 35–0782), implying that partial manganese sites might be occupied by lithium in the spinel lattice. The assumption is supported by ICP-OES measurements. The results showed that the atomic ratio of Li:Mn is 0.578, indicating that a lithium-rich phase of $Li_{1.1}Mn_{1.9}O_4$ is obtained by the reaction between nanotube templates and LiOH at the high temperature. The extra Li^+ in interstitial sites of the lithium-rich manganese oxide improves the structural stability and allows higher Li^+ uptake capacity (Bajestani et al., 2019; Chitrakar et al., 2001; Xiao et al., 2013). It is found that the Brunauer-Emmett-Teller (BET) surface area of LMO nanotubes is 121.3 $m^2 g^{-1}$ (Figure 2), with an average pore size around 50 nm determined by the Barrett-Joyner-Halenda method, which is in good agreement with TEM analysis.

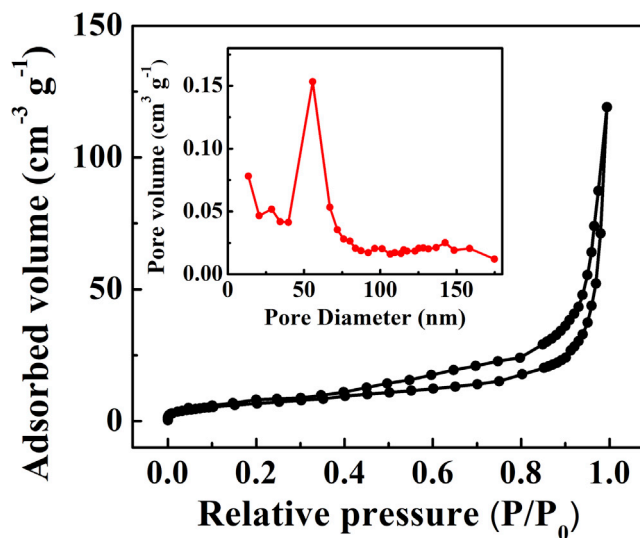


Figure 2. A Nitrogen Adsorption-Desorption Isotherm of Single-Crystalline LMO Nanotubes

The inset shows the corresponding pore size distributions obtained using the Barrett-Joyner-Halenda (BJH) method.

To understand solid-state reactions, we investigated the XRD patterns for the β - MnO_2 nanotube and the calcined products, obtained at 500, 600, and 700°C respectively (Figure 3). The diffraction peaks of nanotube templates are indexed for the tetragonal structure of β - MnO_2 (JCPDS 24–0735, space group $P42/mnm$) without any impurity peaks. Lithium ions enter the square channels of tetragonal β - MnO_2 via solid-state reactions. The reduction of Mn^{IV} to Mn^{III} leads to the lattice expansion owing to the larger radius of Mn^{III} than Mn^{IV} phase, accompanied by the formation of LiO_4 tetrahedra and new MnO_6 octahedra. As XRD results showed, the calcination triggers the reorganization of structure owing to the strongest diffract peak corresponding to (110) reflections of β - MnO_2 disappeared. The transformation is facilitated by the high mobility of Li^+ ions at elevated temperatures (Lu et al., 2019). While LMO500 and LMO600 show the presence of α - Mn_2O_3 phase, an undistorted cubic bixbyite with $Ia3$ symmetry (Figure S3, Supplemental Information); the reaction at 700°C complete phase transformation from tetragonal β - MnO_2 to spinel Li-rich structure. The SEM images of the products prepared at different temperatures showed the nanotube morphology is preserved (Figure S4, Supplemental Information). Despite the impurities were identified at the surface of LMO nanotubes calcined at 500°C (Figures S4A and S4D), the materials show a uniform tubular morphology upon increasing the temperature. The dimension of LMO nanotubes does not change evidently over the solid-state reaction (Figures S4A–S4C). It has been suggested that the tetragonal-to-cubic transformation requires a cooperation jump to a nearest-neighbor site of half the cation array, followed by an adjustment of the Mn-O distances to convert the tetragonal anion packing of rutile to the cubic close packing of anions in the spinel structure (David et al., 1984). The adjustment sustained a minimal reorganization of structure in the tetragonal precursor, generated a more stable spinel LMO framework with a higher symmetry than that of the nanotube templates. Therefore, the tubular nanostructure and high crystallinity of the precursor were preserved through solid-state reactions.

Spinel LMO nanotubes, prepared by β - MnO_2 nanotube and LiOH at 700°C, were selected for Li^+ adsorption/desorption tests followed by the experimental procedure shown in Figure S5 (Supplemental Information). Figure 4A presents the elution curves, accompanied by manganese dissolution, for LMO nanotubes delithiated by 0.5 M H_2SO_4 and $(\text{NH}_4)_2\text{S}_2\text{O}_8$. The results showed that the $(\text{NH}_4)_2\text{S}_2\text{O}_8$ -eluted LMO nanotubes exhibited significantly low manganese dissolution and slightly decreased Li^+ recovery kinetics, as compared to H_2SO_4 -eluted LMO. To elucidate the advantages of single-crystalline nano-tubular structure, we tested the extraction performance of commercial LiMn_2O_4 materials purchased from Aldrich (Figures S6A and S6B, Supplemental Information). The commercial LMO particles exhibit moderate kinetics and low Li^+ uptake capacity (Figure S6C, Supplemental Information), whereas Li^+ uptake capacity of LMO nanotubes was initially high and then steadily reached for an equilibrium. The $(\text{NH}_4)_2\text{S}_2\text{O}_8$ -eluted LMO nanotubes showed low manganese dissolution due to the hydrolysis of $\text{S}_2\text{O}_8^{2-}$, where the peroxy bond breaks into $\text{SO}_4^{\cdot-}$ free radicals (Equation 1) (Marthi and Smith, 2019). The $\text{SO}_4^{\cdot-}/\text{SO}_4^{2-}$ transformation (Equation 2)

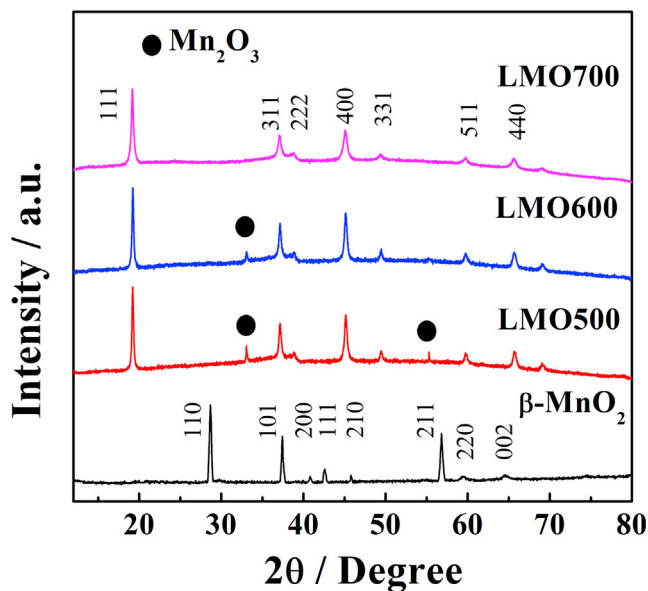
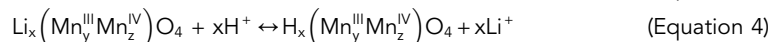
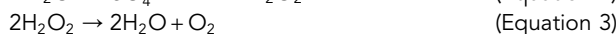
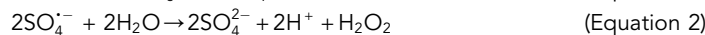


Figure 3. XRD Results of the β - MnO_2 Template and LMO Nanotubes Prepared by Reacting with LiOH for 10 hr at Different Temperatures

LMO500, LMO600, and LMO700 denote a reaction temperature of 500, 600, and 700°C, respectively.

has a high positive reduction potential ($E^\circ = +2.43$ V) compared to $\text{Mn}^{\text{III}}/\text{Mn}^{\text{II}}$ ($E^\circ = +1.54$). As a result, SO_4^{2-} exhibits a higher affinity to accept electrons than Mn^{II} . Therefore, SO_4^{2-} free radicals replace Mn^{III} as an electron acceptor in the $\text{Li}_x(\text{Mn}_y^{\text{III}}\text{Mn}_z^{\text{IV}})\text{O}_4$ framework, inhibiting the reduction of Mn^{III} .



While H^+ acts as an acid extracting Li^+ from LMO nanotubes (Equation 3), the dissolution of manganese could be alleviated due to the generation of O_2 as an oxidant (Equation 4) (Ogino and Oi, 1996). In contrast to commercial LiMn_2O_4 , surface disproportionation might occur in LMO nanotubes due to extra Li^+ in the interstitial sites (Ariza et al., 2006). A hybrid mechanism was involved for Li^+ extraction in LMO nanotubes, containing ion exchange behavior between Li^+ and H^+ and redox extraction of Li^+ . The results of repeated lithium adsorption/desorption tests are shown in Figure 4B. Lithium recovery tests were executed in LiCl solutions using eluted LMO nanotubes. Then, the sorbent was placed in 0.5 M H_2SO_4 or $(\text{NH}_4)_2\text{S}_2\text{O}_8$ to regenerate lithium from adsorbed samples. The manganese dissolution in the nanotube matrix was higher in the first cycle, especially for the H_2SO_4 -treated samples, due to insufficient transformation, Mn^{III} disintegration, and interplanar distance contraction caused by the acidic attack (Gao et al., 2019). The theoretical Li^+ extraction capacity is 43.70 mg g^{-1} based on the composition of $\text{Li}_{1.1}\text{Mn}_{1.9}\text{O}_4$. The $(\text{NH}_4)_2\text{S}_2\text{O}_8$ -eluted LMO nanotubes registered a recovery capacity of 39.21 mg g^{-1} with a capacity retention of 86.73% after regeneration, whereas the capacity retention of H_2SO_4 -eluted LMO is only 69.67%. Meanwhile, the recovery capacity of H_2SO_4 -eluted LMO was sharply decreased during adsorption/desorption cycling, compared to LMO nanotubes eluted by $(\text{NH}_4)_2\text{S}_2\text{O}_8$. After the eight cycles, LMO nanotubes obtained from $(\text{NH}_4)_2\text{S}_2\text{O}_8$ eluent exhibited a recovery capacity of 23.96 mg g^{-1} and corresponding Mn dissolution of 0.12%, while H_2SO_4 -eluted LMO nanotubes showed a recovery capacity of 10.96 mg g^{-1} and H_2SO_4 -eluted commercial LMO failed to function (Figure S6D, Supplemental Information).

XRD patterns of pristine LMO and LMO nanotubes, eluted by H_2SO_4 and $(\text{NH}_4)_2\text{S}_2\text{O}_8$, after cycling tests were shown in Figure 4C. It is observed that the spinel structure of LMO nanotubes was preserved for both H_2SO_4 -eluted and $(\text{NH}_4)_2\text{S}_2\text{O}_8$ -eluted LMO nanotubes. As the peak shift toward higher 2θ values is observed upon delithiation, retention of the spinel structure indicates lithium desorption proceeds

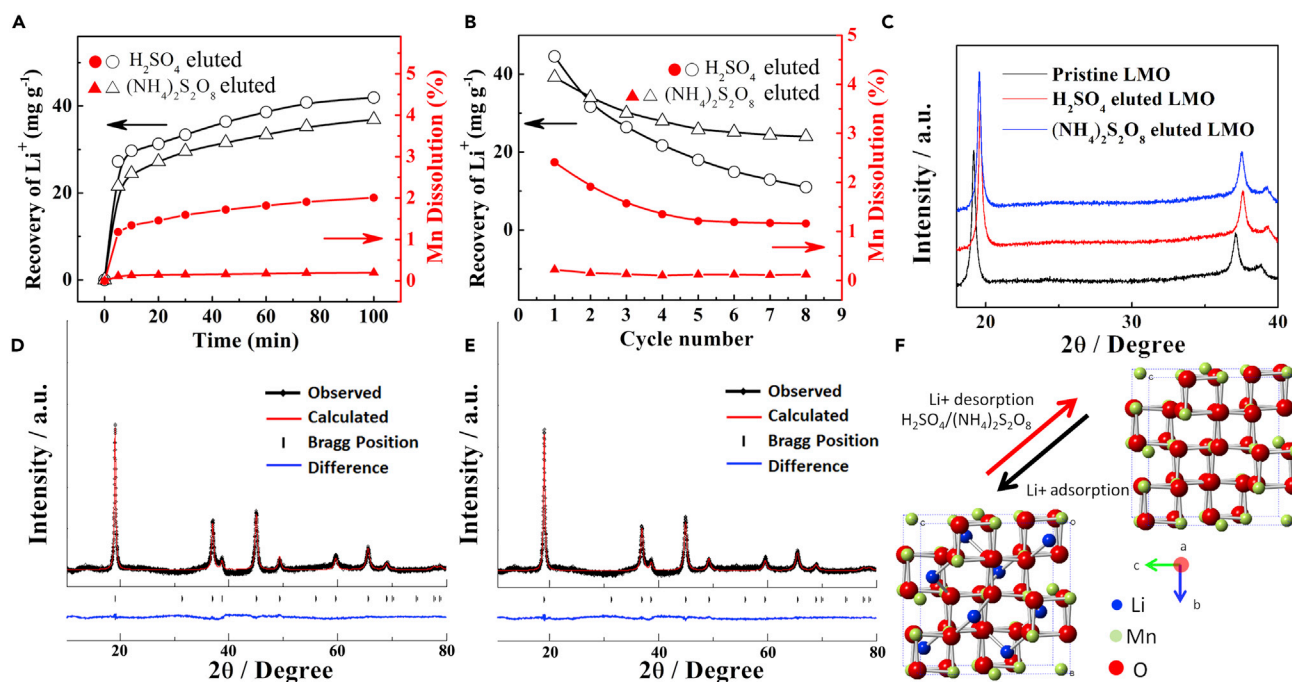


Figure 4. Extraction and Recovery Performance of LMO Nanotubes

(A and B) (A) Elution tests and (B) regeneration tests of Li extraction, along with Mn dissolution, for LMO nanotubes eluted by 0.5 M H₂SO₄ and (NH₄)₂S₂O₈. (C–E) (C) XRD results of pristine LMO, H₂SO₄-eluted, and (NH₄)₂S₂O₈-eluted LMO nanotubes, respectively. Rietveld refinement of (D) H₂SO₄-eluted and (E) (NH₄)₂S₂O₈-eluted LMO nanotubes after eight adsorption/desorption cycles. (F) Schematic illustration of the lithium uptake for adsorption/desorption processes.

topotactically. Rietveld refinements were used to analyze the XRD results of H₂SO₄-eluted and (NH₄)₂S₂O₈-eluted LMO nanotubes (Figures 4D and 4E). LMO nanotubes, eluted by 0.5 M H₂SO₄ and (NH₄)₂S₂O₈, exhibit a lattice parameter of 8.032 and 8.054 Å, respectively, indicating a larger volume change for H₂SO₄-eluted LMO nanotubes (Table 1). While the pristine LMO showed a Li-rich spinel structure after solid-state reactions, the ratio of Li/Mn is reduced due to Mn dissolution after eight adsorption/desorption cycles (Table 1). It has been known that adequate Mn^{III}/Mn^{IV} ions in the spinel structure are necessary to maintain the ideal cubic dense packing state of O atoms in each layer, forming a Mn₂O₄ skeleton which is favorable for Li⁺ diffusion (Figure 4F) (Ben et al., 2017). The Li⁺ extraction at the 8a position of the LMO through the path of 8a–16c–8a. The Jahn-Teller effect may occur during the adsorption/desorption process that the repeated insertion/extraction of Li⁺ causes the deformation and even collapse of the spinel structure (Ragavendran et al., 2017).

Figure 5A showed that X-Ray Photoelectron Spectroscopy (XPS) spectra of Mn 2p_{1/2} and Mn 2p_{3/2} for pristine LMO and LMO nanotubes, eluted by H₂SO₄ and (NH₄)₂S₂O₈. The shift of binding energy is attributed to the lattice distortion of manganese-oxygen bonds (Qian et al., 2020). The valence analysis was performed by deconvolutions of Mn 2p_{3/2} spectra (Figure 5B). The results indicated that the ratios of Mn⁴⁺:Mn³⁺ on the surface are 51.0%:49.0%, 44.9%:55.1%, and 46.8%:53.2% for pristine LMO, H₂SO₄-eluted, and (NH₄)₂S₂O₈-eluted LMO nanotubes, respectively (Table 1). While eluted LMO nanotubes exhibit an increase of Mn³⁺, (NH₄)₂S₂O₈-eluted LMO nanotubes showed higher valence state of Mn compared to H₂SO₄-eluted LMO nanotubes. The reduction of Mn triggered dissolutions of Mn²⁺ in acid solutions during the extraction process (Gao et al., 2018). It is suggested that as the average valence state of Mn decreased lower than +3.5, the cubic crystal changes to tetragonal, while the tetragonal phase showed irreversible transformations of Li⁺ adsorption/desorption (Abuzeid et al., 2018). The improved recovery performance of LMO nanotubes is attributed to higher chemical stability and less volume changes for the acid-free processing.

The acid-free method was employed for Li⁺ recovery from simulated brines. (NH₄)₂S₂O₈-eluted LMO nanotubes exhibited a high selectivity of Li⁺ from the brine, containing Li⁺, Na⁺, K⁺, and Mg²⁺ ions under the

	Pristine LMO	LMO Recycled by H ₂ SO ₄	LMO Recycled by (NH ₄) ₂ S ₂ O ₈
a (Å)	8.239	8.032	8.054
V (Å ³)	559.27	518.17	522.44
Crystallite size (nm)	12.52	15.17	14.72
R _{wp} (%)	2.83	3.48	3.12
Mn ⁴⁺ (%):Mn ³⁺ (%)	51.0:49.0	44.9:55.1	46.8:53.2
Li:Mn ratio	0.578	0.513	0.572

Table 1. Rietveld Refinement Results, Mn Valence, and Li:Mn Ratio for Different Materials

Li:Mn ratio was obtained from ICP-OES tests. Mn Valence was analyzed by XPS measurements.

same batch condition (Figure S7A Supplemental Information). The concentration of cations plays an important role in the adsorption behavior of nanotubes. Considering the extremely unbalance ratio was detected in salt lakes, the adsorption capacity of (NH₄)₂S₂O₈-eluted LMO nanotubes was tested using brines with different Li⁺:Na⁺ ratios. As shown in Figure S7B (Supplemental Information), (NH₄)₂S₂O₈-eluted LMO nanotubes retain 88.32% of adsorption capacity with good Li⁺ recognition ability when Li⁺:Na⁺ ratio is increased from 1:1 to 1:10. Further increase of the brine concentrations results in the presence of white crystals, ascribed to the unabsorbed salts (Figure S8, Supplemental Information). The adsorption performance was briefly summarized and compared with previous studies (Table S1, Supplemental Information). The results demonstrated that single-crystalline nanotubes deliver excellent adsorption capacity and the highest extraction efficiency with respect to the theoretical capacity of adsorption. Thus, the acid-free strategy is promising for practical applications of lithium extraction.

DISCUSSION

With the surging demand for lithium, it is necessary to develop new technologies for lithium extraction with high efficiency and good reusability. In this work, we developed a new strategy for nano-extraction of lithium, based on single-crystalline LMO nanotubes recycled by (NH₄)₂S₂O₈ as an eluent. The promising Li⁺ recovery performance of LMO nanotubes is attributed to their novel architecture and single-crystalline structure. The LMO nanotubes obtained via template-engaged reaction can serve as channels for lithium-ion adsorption/desorption, whereas the hollow nanostructure of spinel LMO may act as reservoirs for the lithium uptake. The limitation of internal pore diffusion could be overcome by the tubular morphology, consequently leading to a sufficient adsorbent-solution interface to absorb Li⁺ and promote rapid ion transportation. While nano-sized holes in LMO nanotubes can supply facile transport channels with short length for lithiation, a single-crystalline structure can reduce the transport resistance of lithium ions. On the other hand, LMO materials suffer from performance degradations due to manganese dissolutions and irreversible volume changes in the conventional acidic elution process. (NH₄)₂S₂O₈ eluent ensures the structural stability of LMO nanotubes by improving the reversibility of Li⁺ recovery and buffering the volume change, attributed to Jahn-Teller effects. The method developed in this investigation can be used for the synthesis and modifications of LMO materials for various applications such as battery recycling and lithium-ion sieve fabrications.

Overall, we successfully demonstrated a nano-extraction approach, based on LMO nanotubes as the adsorbent and (NH₄)₂S₂O₈ as the eluent. Spinel LMO nanotubes were synthesized via a template-engaged reaction using β-MnO₂ nanotubes as the precursor, in which the tubular morphology and single-crystal characteristics of LMO nanotubes can be preserved due to minimal structure reconstruction during the phase transformation. As the sorbent for lithium recovery, the LMO nanotubes exhibited favorable extraction performance, which may be attributed to their unique tubular nanostructures, single-crystalline nature, and high crystallinity. The manganese dissolution in the acidic environment has been overcome by using (NH₄)₂S₂O₈ for lithium recovery. (NH₄)₂S₂O₈ eluent improves recovery performance and cycling stability of LMO nanotubes compared to that eluted by H₂SO₄. The acid-free extraction ensures the reusability, selectivity, and recovery properties for spinel LMO materials.

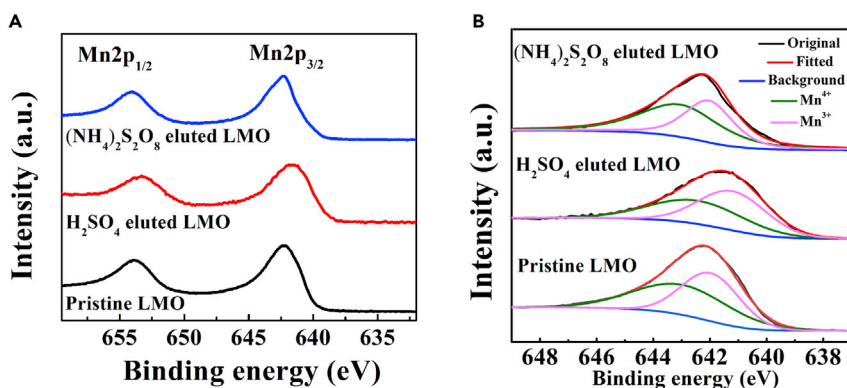


Figure 5. Surface Valence Analysis of LMO Nanotubes

XPS results of (A) Mn $2p_{1/2}$ and Mn $2p_{3/2}$ spectra and (B) deconvoluted profile of specific Mn $2p_{3/2}$ spectra for pristine LMO, H_2SO_4 -eluted, and $(\text{NH}_4)_2\text{S}_2\text{O}_8$ -eluted LMO nanotubes, respectively

Limitations of the Study

Here, we proposed single-crystalline LMO nanotubes, synthesized by a template-engaged method, for lithium extractions. The degradation of LMO nanotubes has been overcome using $(\text{NH}_4)_2\text{S}_2\text{O}_8$ as the eluent, which reduced manganese dissolutions and improved capacity retention upon adsorption/desorption processes. The marriage of LMO nanotubes and $(\text{NH}_4)_2\text{S}_2\text{O}_8$ allows $\sim 89.73\%$ theoretical capacity of the sorbent in pure LiCl solutions. However, for lithium recovery from real brines, efficiency and adsorption behavior need to be optimized according to in-service conditions. For those containing highly concentrated Na^+ and Mg^{2+} , recovery practices should be integrated with pre-treatments, such as filtration, evaporation, and participation.

Resource Availability

Lead Contact

Further information and requests for resources should be directed to the Lead Contact, Kaiyuan Shi (shiky7@mail.sysu.edu.cn).

Materials Availability

The materials that support the findings of this study are available from the corresponding author upon reasonable request.

Data and Code Availability

This study did not generate/analyze data sets/code.

METHODS

All methods can be found in the accompanying [Transparent Methods supplemental file](#).

SUPPLEMENTAL INFORMATION

Supplemental Information can be found online at <https://doi.org/10.1016/j.isci.2020.101768>.

ACKNOWLEDGMENTS

K.S. is thankful for the Research Start-up Funds from Sun Yat-sen University (29000-18841231). J.Y. acknowledges support from the Fundamental Research Funds for the Central Universities (2019py77) and Guangdong Basic & Applied Basic Research Foundation (No. 2019A1515110436). Z.X. is grateful for the funding from the Education Department of Guangdong Province (2018KQNCX059) and Guangdong Basic & Applied Basic Research Foundation (No. 2020A1515011549). The authors would like to thank R. Niu from the Shiyanjia Lab (www.shiyanjia.com) for XPS tests.

AUTHOR CONTRIBUTIONS

K.S. conceived the idea and managed the project. M.L., J.Y., S.Z., Z.X., and R.C. performed the experiments. K.S. and Z.X. analyzed the results and wrote the paper. All authors discussed the results and contributed to the manuscript.

DECLARATION OF INTERESTS

The authors declare no competing interests.

Received: July 28, 2020

Revised: October 15, 2020

Accepted: October 30, 2020

Published: November 20, 2020

REFERENCES

- Abuzeid, H.M., Hashem, A.M., Kaus, M., Knapp, M., Indris, S., Ehrenberg, H., Mauger, A., and Julien, C.M. (2018). Electrochemical performance of nanosized MnO₂ synthesized by redox route using biological reducing agents. *J. Alloys Comp.* **746**, 227–237.
- Ariza, M.J., Jones, D.J., Rozière, J., Chitrakar, R., and Ooi, K. (2006). Probing the local structure and the role of protons in lithium sorption processes of a new lithium-rich manganese oxide. *Chem. Mater.* **18**, 1885–1890.
- Bajestani, M.B., Moheb, A., and Masigol, M. (2019). Simultaneous optimization of adsorption capacity and stability of hydrothermally synthesized spinel ion sieve composite adsorbents for selective removal of lithium from aqueous solutions. *Ind. Eng. Chem. Res.* **58**, 12207–12215.
- Battistel, A., Palagonia, M.S., Brogioli, D., La Mantia, F., and Trocoli, R. (2020). Electrochemical methods for lithium recovery: a comprehensive and critical review. *Adv. Mater.* **32**, e1905440.
- Ben, L., Yu, H., Chen, B., Chen, Y., Gong, Y., Yang, X., Gu, L., and Huang, X. (2017). Unusual spinel-to-layered transformation in LiMn₂O₄ cathode explained by electrochemical and thermal stability investigation. *ACS Appl. Mater. Interfaces* **9**, 35463–35475.
- Biswal, B.K., Jadhav, U.U., Madhaiyan, M., Ji, L., Yang, E.-H., and Cao, B. (2018). Biological leaching and chemical precipitation methods for recovery of Co and Li from spent lithium-ion batteries. *ACS Sust. Chem. Eng.* **6**, 12343–12352.
- Chitrakar, R., Kanoh, H., Miyai, Y., and Ooi, K. (2001). Recovery of lithium from seawater using manganese oxide adsorbent (H_{1.6}Mn_{1.6}O₄) derived from Li_{1.6}Mn_{1.6}O₄. *Ind. Eng. Chem. Res.* **40**, 2054–2058.
- Choi, S., Hwang, G., Ilyas, S., Han, Y., Myung, N.V., Lee, B.-c., Song, Y., and Kim, H. (2020). Inorganic nanofiber as a promising sorbent for lithium recovery. *Sep. Purif. Technol.* **242**, 116757.
- David, W.I.F., Thackeray, M.M., Bruce, P.G., and Goodenough, J.B. (1984). Lithium insertion into βMnO₂ and the rutile-spinel transformation. *Mater. Res. Bull.* **19**, 99–106.
- Ding, Y.-L., Xie, J., Cao, G.-S., Zhu, T.-J., Yu, H.-M., and Zhao, X.-B. (2011). Single-crystalline LiMn₂O₄ nanotubes synthesized via template-engaged reaction as cathodes for high-power lithium ion batteries. *Adv. Funct. Mater.* **21**, 348–355.
- Du, X., Guan, G., Li, X., Jagadale, A.D., Ma, X., Wang, Z., Hao, X., and Abudula, A. (2016). A novel electroactive λ-MnO₂/PPy/PSS core-shell nanorod coated electrode for selective recovery of lithium ions at low concentration. *J. Mater. Chem. A* **4**, 13989–13996.
- Gao, A., Hou, X., Sun, Z., Li, S., Li, H., and Zhang, J. (2019). Lithium-desorption mechanism in LiMn₂O₄, Li_{1.33}Mn_{1.67}O₄, and Li_{1.6}Mn_{1.6}O₄ according to precisely controlled acid treatment and density functional theory calculations. *J. Mater. Chem. A* **7**, 20878–20890.
- Gao, A., Sun, Z., Li, S., Hou, X., Li, H., Wu, Q., and Xi, X. (2018). The mechanism of manganese dissolution on Li_{1.6}Mn_{1.6}O₄ ion sieves with HCl. *Dalton Trans.* **47**, 3864–3871.
- Hayashi, F., Kurokawa, S., Shiiba, H., Wagata, H., Yubuta, K., Oishi, S., Nishikiori, H., and Teshima, K. (2016). Exceptional flux growth and chemical transformation of metastable orthorhombic LiMnO₂ cuboids into hierarchically-structured porous H_{1.6}Mn_{1.6}O₄ rods as Li ion sieves. *Cryst. Growth Des.* **16**, 6178–6185.
- Hong, H.-J., Ryu, T., Park, I.-S., Kim, M., Shin, J., Kim, B.-G., and Chung, K.-S. (2018). Highly porous and surface-expanded spinel hydrogen manganese oxide (HMO)/Al₂O₃ composite for effective lithium (Li) recovery from seawater. *Chem. Eng. J.* **337**, 455–461.
- Kamran, U., Heo, Y.-J., Lee, J.W., and Park, S.-J. (2019). Chemically modified activated carbon decorated with MnO₂ nanocomposites for improving lithium adsorption and recovery from aqueous media. *J. Alloys Comp.* **794**, 425–434.
- Li, L., Zhang, X., Li, M., Chen, R., Wu, F., Amine, K., and Lu, J. (2018). The recycling of spent lithium-ion batteries: a review of current processes and technologies. *Electrochem. Energy Rev.* **1**, 461–482.
- Lin, H., Yu, X., Li, M., Duo, J., Guo, Y., and Deng, T. (2019). Synthesis of polyporous ion-sieve and its application for selective recovery of lithium from geothermal water. *ACS Appl. Mater. Interfaces* **11**, 26364–26372.
- Liu, G., Zhao, Z., and Ghahreman, A. (2019). Novel approaches for lithium extraction from salt-lake brines: a review. *Hydrometallurgy* **187**, 81–100.
- Lu, F., Pang, Y., Zhu, M., Han, F., Yang, J., Fang, F., Sun, D., Zheng, S., and Wang, C. (2019). A high-performance Li–B–H electrolyte for all-solid-state Li batteries. *Adv. Funct. Mater.* **29**, 1809219.
- Luo, X., Zhang, K., Luo, J., Luo, S., and Crittenden, J. (2016). Capturing lithium from wastewater using a fixed bed packed with 3-D MnO₂ ion cages. *Environ. Sci. Technol.* **50**, 13002–13012.
- Marthi, R., and Smith, Y.R. (2019). Selective recovery of lithium from the Great Salt Lake using lithium manganese oxide-diatomaceous earth composite. *Hydrometallurgy* **186**, 115–125.
- Moazeni, M., Hajipour, H., Askari, M., and Nusheh, M. (2015). Hydrothermal synthesis and characterization of titanium dioxide nanotubes as novel lithium adsorbents. *Mater. Res. Bull.* **61**, 70–75.
- Ogino, H., and Oi, T. (1996). Extraction of lithium from LiMn₂O₄ by ammonium peroxodisulfate and lithium isotope selectivities of adsorbents thus obtained. *Sep. Sci. Technol.* **31**, 1215–1231.
- Ooi, K., Sonoda, A., Makita, Y., Chitrakar, R., Tasaki-Handa, Y., and Nakazato, T. (2017). Recovery of lithium from salt-brine eluates by direct crystallization as lithium sulfate. *Hydrometallurgy* **174**, 123–130.
- Paranthaman, M.P., Li, L., Luo, J., Hoke, T., Ucar, H., Moyer, B.A., and Harrison, S. (2017). Recovery of lithium from geothermal brine with lithium–aluminum layered double hydroxide chloride sorbents. *Environ. Sci. Technol.* **51**, 13481–13486.
- Pasta, M., Battistel, A., and La Mantia, F. (2012). Batteries for lithium recovery from brines. *Energy Environ. Sci.* **5**, 9487.
- Qian, F., Zhao, B., Guo, M., Li, J., Liu, Z., and Wu, Z. (2020). K-gradient doping to stabilize the spinel structure of Li_{1.6}Mn_{1.6}O₄ for Li⁺ recovery. *Dalton Trans.* **49**, 10939–10948.
- Ragavendran, K., Xia, H., Mandal, P., and Arof, A.K. (2017). Jahn–Teller effect in LiMn₂O₄: influence on charge ordering, magnetoresistance and battery performance. *Phys. Chem. Chem. Phys.* **19**, 2073–2077.

Safari, S., Lottermoser, B.G., and Alessi, D.S. (2020). Metal oxide sorbents for the sustainable recovery of lithium from unconventional resources. *Appl. Mater. Today* *19*, 100638.

Tang, L., Huang, S., Wang, Y., Liang, D., Li, Y., Li, J., Wang, Y., Xie, Y., and Wang, W. (2020). Highly efficient, stable, and recyclable hydrogen manganese oxide/cellulose film for the extraction of lithium from seawater. *ACS Appl. Mater. Interfaces* *12*, 9775–9781.

Tang, W., Hou, Y., Wang, F., Liu, L., Wu, Y., and Zhu, K. (2013). LiMn₂O₄ nanotube as cathode material of second-level charge capability for aqueous rechargeable batteries. *Nano Lett.* *13*, 2036–2040.

Trócoli, R., Erinmwingbovo, C., and LaMantia, F. (2017). Optimized lithium recovery from brines by

using an electrochemical ion-pumping process based on λ -MnO₂ and nickel hexacyanoferrate. *ChemElectroChem* *4*, 143–149.

Wang, H., Cui, J., Li, M., Guo, Y., Deng, T., and Yu, X. (2020). Selective recovery of lithium from geothermal water by EGDE cross-linked spherical CTS/LMO. *Chem. Eng. J.* *389*, 124410.

Wei, S., Wei, Y., Chen, T., Liu, C., and Tang, Y. (2020). Porous lithium ion sieves nanofibers: general synthesis strategy and highly selective recovery of lithium from brine water. *Chem. Eng. J.* *379*, 122407.

Wu, Z., and Zhao, D. (2011). Ordered mesoporous materials as adsorbents. *Chem. Commun. (Camb.)* *47*, 3332–3338.

Xiao, J.-L., Sun, S.-Y., Wang, J., Li, P., and Yu, J.-G. (2013). Synthesis and adsorption properties of Li_{1.6}Mn_{1.6}O₄ spinel. *Ind. Eng. Chem. Res.* *52*, 11967–11973.

Xu, X., Chen, Y., Wan, P., Gasem, K., Wang, K., He, T., Adidharma, H., and Fan, M. (2016). Extraction of lithium with functionalized lithium ion-sieves. *Prog. Mater. Sci.* *84*, 276–313.

Zhang, G., Zhang, J., Zhou, Y., Qi, G., Wu, Y., Hai, C., and Tang, W. (2019). Synthesis of aluminum-doped ion-sieve manganese oxides powders with enhanced adsorption performance. *Colloids Surf. A Physicochem. Eng. Asp.* *583*, 123950.

Zhang, L., Li, L., Rui, H., Shi, D., Peng, X., Ji, L., and Song, X. (2020). Lithium recovery from effluent of spent lithium battery recycling process using solvent extraction. *J. Hazard. Mater.* *398*, 122840.

iScience, Volume 23

Supplemental Information

Extraction of Lithium from Single-Crystalline

Lithium Manganese Oxide Nanotubes

Using Ammonium Peroxodisulfate

Kaiyuan Shi, Mingwu Luo, Jie Ying, Shunying Zhen, Zhenyu Xing, and Ri Chen

Transparent Methods

Preparation of single-crystalline LMO nanotubes

Spinel-type LMO nanotubes were prepared by β -MnO₂ nanotube templates by a modified hydrothermal process. In this method, MnSO₄·H₂O (40 mmol) and PVP (45 mmol, K30) were dissolved in deionized water (100 mL). Then, 40 mL NaClO₃ (1 M) solution was added to the above solution under continuous stirring. The mixed solution was transferred to a Teflon-lined stainless steel autoclave and heated at 180°C for 10 h. The black precipitate was filtered and washed with deionized water and ethanol, and subsequently dried in a vacuum oven. The as-prepared β -MnO₂ was mixed with LiOH·H₂O at a molar ratio of 1.9:1.1 (with an extra ~5% LiOH·H₂O) and dispersed into 10 mL methanol to form a homogenous slurry, and then dried at the room temperature overnight. The mixture was calcined in a range of 500-700 °C for 10 h to obtain spinel LMO nanotubes.

Characterization of Materials

The crystallographic structure was studied by the X-ray diffraction (XRD) method, operated on a powder diffractometer (NicoletI2, monochromatized CuK- α radiation). The obtained patterns were refined by the TOPAS program using the Rietveld method, with ICSD crystallographic information as references for the refinements (Majzoub and Rönnebro, 2012). The BET specific surface area and pore size distribution were acquired using the nitrogen adsorption/desorption method by Quantachrome Autosorb-1 equipment. The microstructure was investigated by Hitachi SU5000 scanning electron microscope (SEM) and FEI Tecnai Osiris Transmission electron microscopy (TEM). The concentration of metal ions in the solution was determined by an inductively coupled

plasma-optical emission spectroscopy (ICP-OES, Thermo Jarrell Ash IRIS Advantage). The surface chemistry and the valence state of Mn were studied using X-ray photoelectron spectroscopy (XPS, Thermo Scientific K-Alpha).

Lithium extraction/recovery tests

Lithium adsorption/desorption performance was studied in a batch system as shown in Figure S5. The obtained powders were firstly delithiated in the eluent until the extraction of lithium reached equilibrium. The lithium recovery experiments were conducted in 0.1 M LiCl solutions at 60°C. The pH of LiCl solutions was adjusted to 8 using 1 M LiOH. The recovery of lithium was carried out by stirring 1 g HMO powders in 40 ml of lithium solutions for 4 h. For the desorption tests, the sorbent was stirred in a 0.5 M H₂SO₄ or (NH₄)₂S₂O₈ solution for 4 h. Sorbent–sorbate mixture was analyzed after centrifuged at 3500 rpm for 10 min, followed by washing with DI water to remove the residues. The Li⁺ selectivity tests were carried out using 1 g (NH₄)₂S₂O₈-eluted LMO nanotubes in 40 mL in simulated brines. The brines contain 0.05 M LiCl, KCl and MgCl₂, and NaCl in different concentrations of 0.05-0.5 M. The concentrations of Li⁺ and coexisting cations in all solutions were determined at intervals by the ICP-OES. The adsorption capacity was calculated by $q_e = \Delta C * V / m$, where ΔC is the change of Li⁺ concentration (mg L⁻¹); V is solution volume (L); and m is sorbent mass (g), respectively. The adsorption capacity was reported based on the average value calculation for three samples.

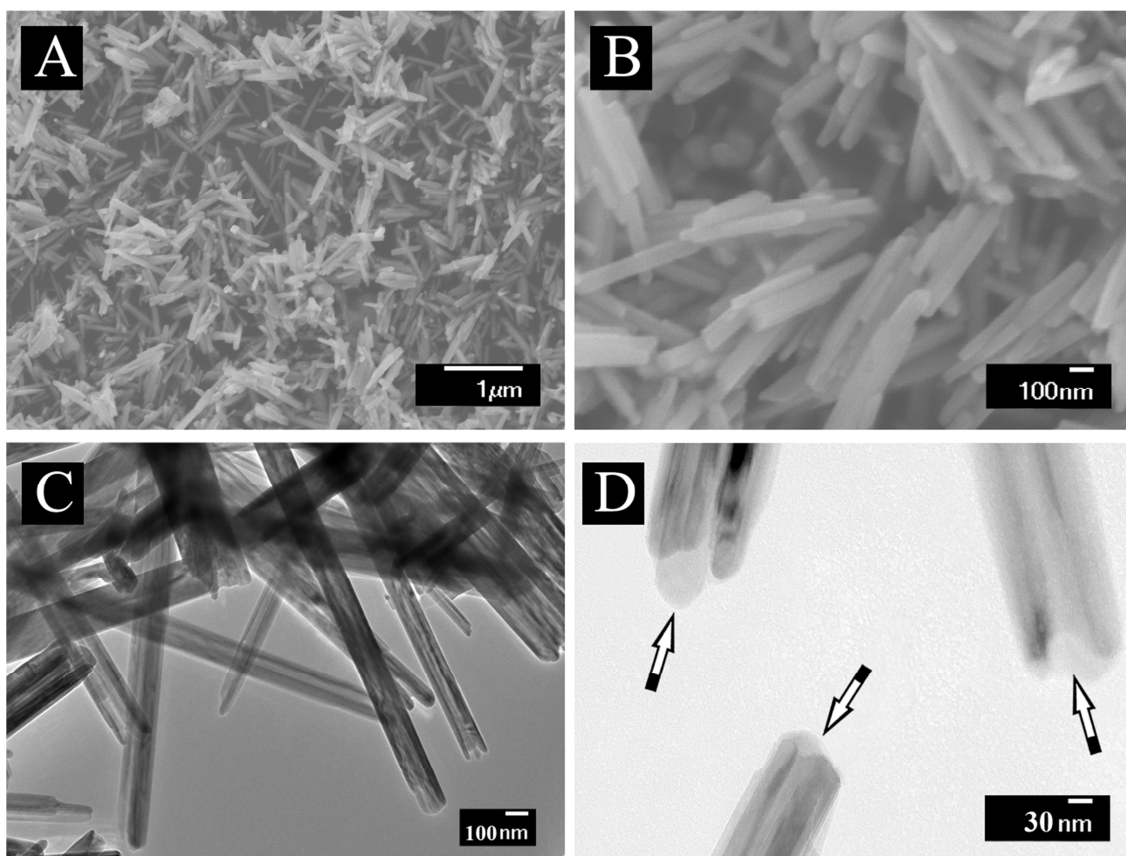


Figure S1 A, B) SEM and C, D) TEM images of β -MnO₂ nanotube templates, obtained from a hydrothermal process, at different magnifications. The arrows in (D) show the tip with an interior hollow structure of individual tubes. Related to Figure 1.

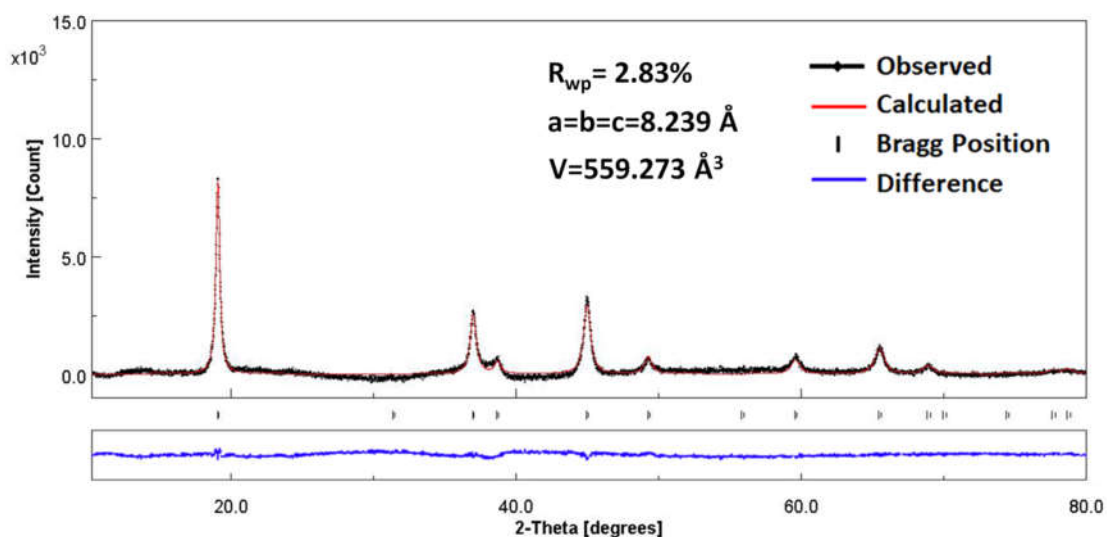


Figure S2 Rietveld refinement results of LMO nanotubes, prepared by a solid-state reaction between $\beta\text{-MnO}_2$ nanotube templates and $\text{LiOH}\cdot\text{H}_2\text{O}$ at $700 \text{ }^\circ\text{C}$ for 10 h. The pattern was refined using a single-phase model with the $Fd\bar{3}m$ symmetry; in this structure, lithium, manganese and oxygen reside on the $8a$ (tetrahedral), $16d$ (octahedral), and $32e$ Wyckoff sites, respectively. The instrumental resolution function was determined by fitting the XRD pattern of a standard powder sample LaB_6 (Britto and Kamath, 2014). Related to Figure 1.

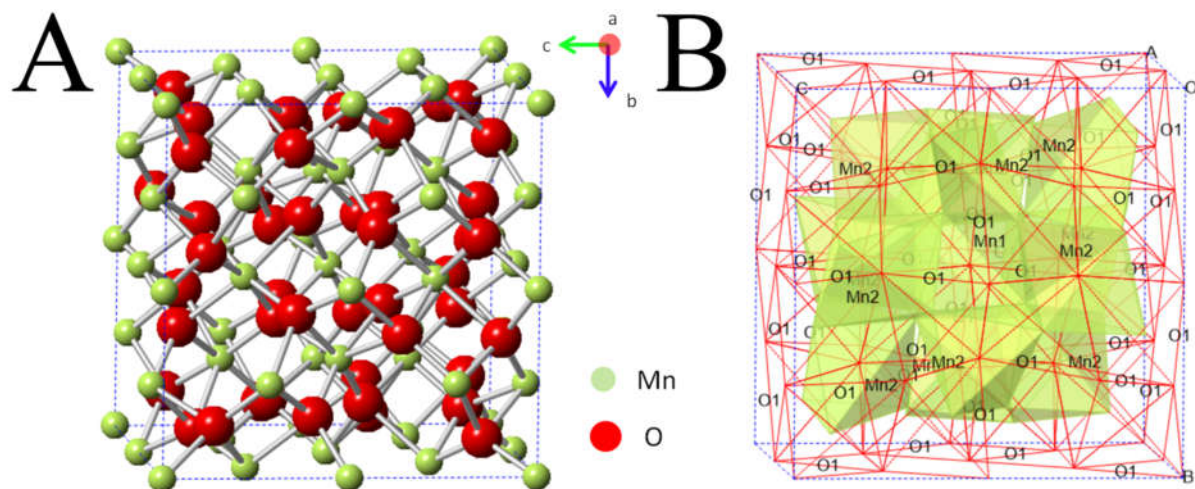


Figure S3 Crystal structure of α - Mn_2O_3 (Bixbyite JCPDS 41-1442, $Ia-3$ structure), formed by a solid-state reaction between β - MnO_2 templates and $\text{LiOH}\cdot\text{H}_2\text{O}$ within a range of 500-600 °C, in the view of A) atom and B) polyhedral model. Related to Figure 3.

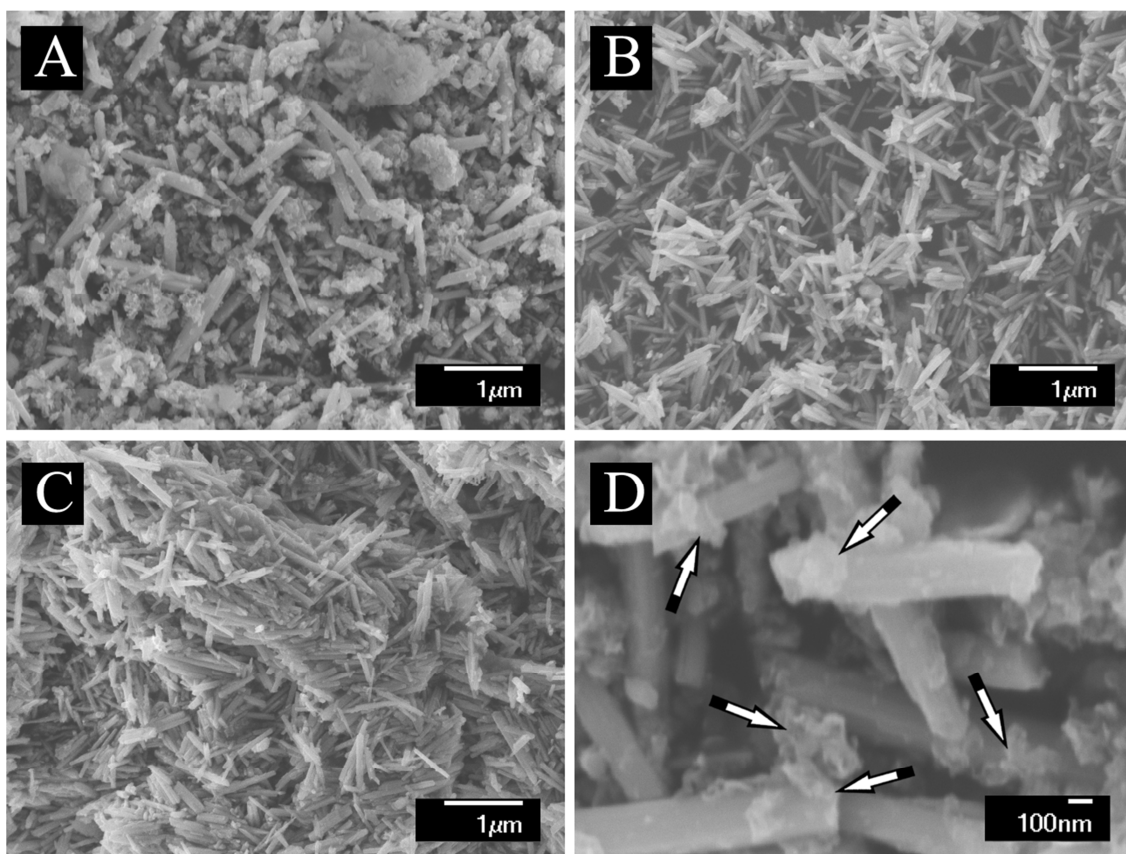


Figure S4 SEM images of the products derived from a solid-state reaction between β -MnO₂ nanotube templates and LiOH·H₂O at different temperatures for 10 h: A) 500 °C, B) 600 °C, C) 700°C, and D) the magnified view of A). The arrows in (D) show the impurities corresponding to α -Mn₂O₃ phase (JCPDS 41-1442). Related to Figure 3.

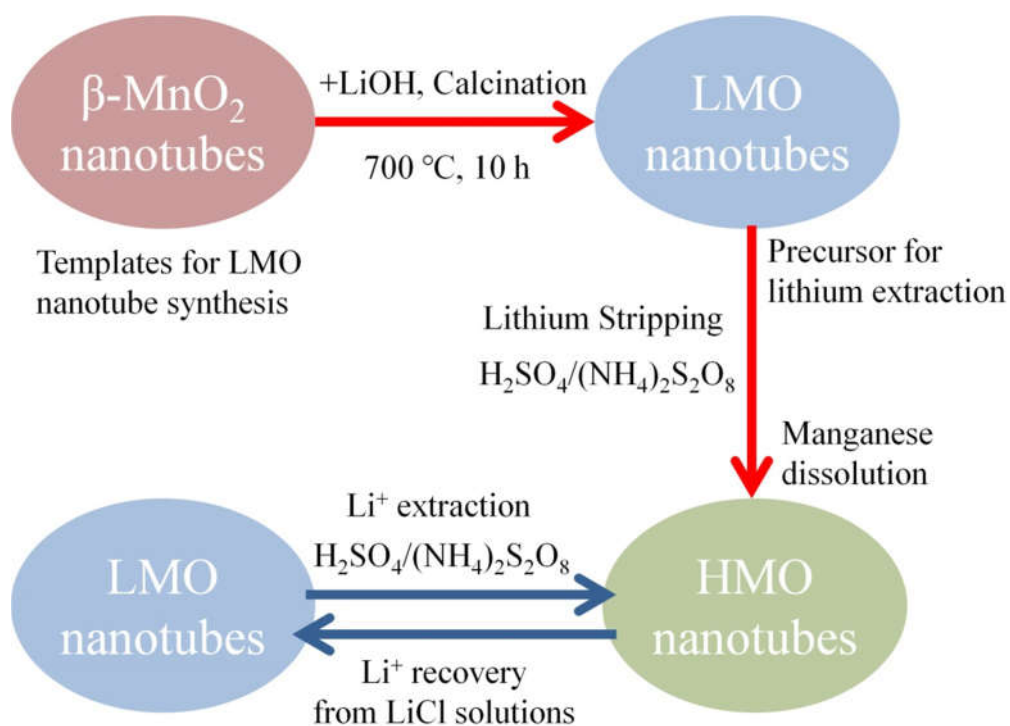


Figure S5 Scheme of experimental procedures for LMO nanotube synthesis and Li⁺ adsorption/desorption tests. Related to Figure 4.

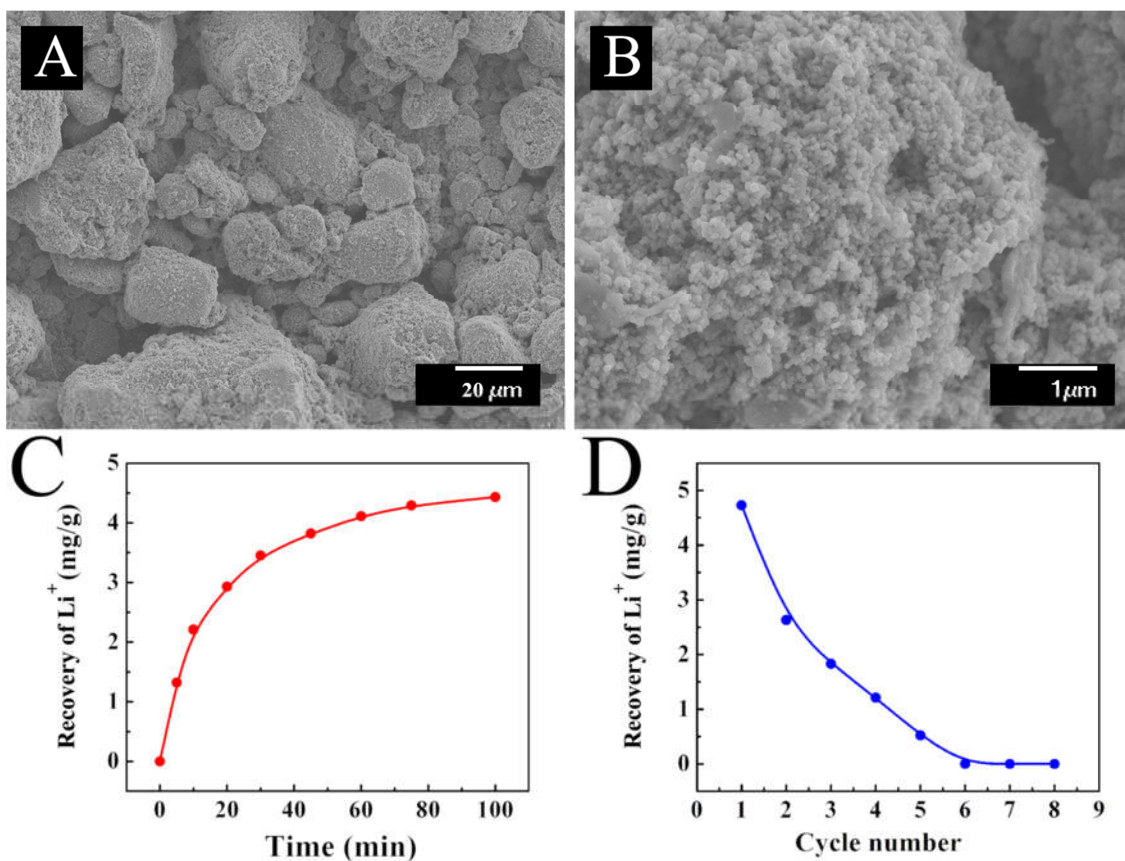


Figure S6 A, B) SEM images of commercial LiMn_2O_4 materials at different magnifications and C) elution test and D) regeneration test results of Li extraction for commercial LiMn_2O_4 materials, delithiated using $0.5 \text{ H}_2\text{SO}_4$. The tests were carried out at the temperature of 60°C and pH of 8, adjusted by 1 M LiOH . The spinel LiMn_2O_4 materials from Sigma-Aldrich (Stock# 725129) were investigated because of its wide availability. SEM image shows the materials are heterogeneous with a broad size distribution in the micron-size. The initial (C_0) and final (C_1) concentrations of Li^+ solutions were measured by ICP-OES tests. The Li^+ recovery capacity (Q) was obtained based on the change of Li^+ concentration. Related to Figure 4.

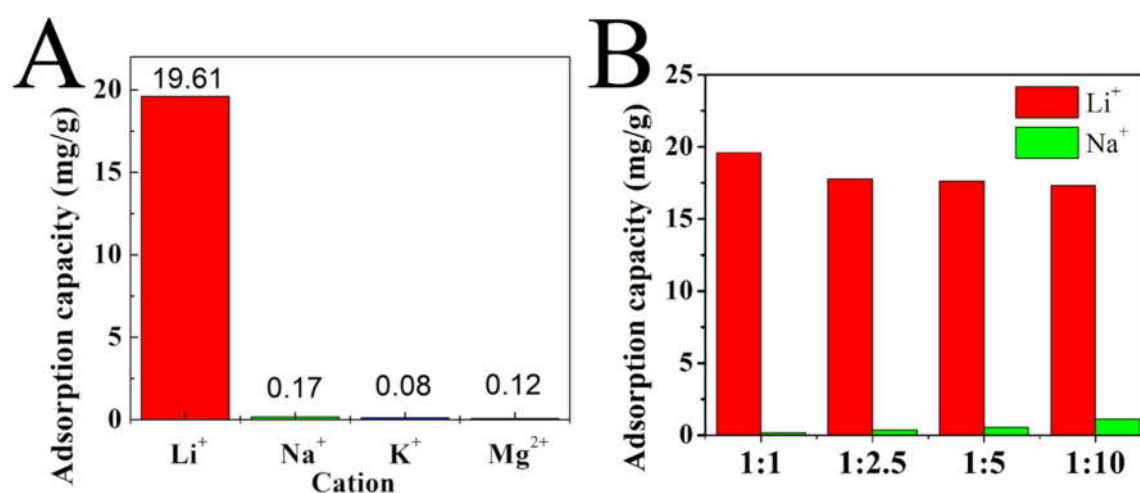


Figure S7 Recovery behavior of $(\text{NH}_4)_2\text{S}_2\text{O}_8$ -eluted LMO nanotubes in simulated brines: A) competitive cation uptakes tested at 0.05 mol L^{-1} Li^+ , Na^+ , K^+ , and Mg^{2+} and B) adsorption performance at different $\text{Na}^+:\text{Li}^+$ ratios. Related to Figure 4 and Table 1.

For practical applications of lithium recovery from brines, Li^+ -containing mother liquors may carry various cations, such as Na^+ , K^+ , and Mg^{2+} ions, etc (Marthi and Smith, 2019; Ryu et al., 2016). Therefore it is essential to investigate the influence of coexisting ions on the adsorption performance of LMO nanotubes. The selectivity tests were carried out using simulated brines containing LiCl , NaCl , KCl and MgCl_2 . 1 g $(\text{NH}_4)_2\text{S}_2\text{O}_8$ -eluted LMO nanotube was dispersed in 40 ml of the brine at 60°C for 4 h. The concentrations of each ion were measured using ICP-OES before and after extraction tests. Simulated brines exhibited lower Li^+ uptake capacity compared to LiCl solutions, indicating Li^+ adsorption was regulated by cation concentrations. $(\text{NH}_4)_2\text{S}_2\text{O}_8$ -eluted nanotubes showed a high selectivity of Li^+ as the adsorption capacity of Li^+ is two orders higher, compared to that of Na^+ , K^+ , and Ca^{2+} (Figure S7A). The Li^+ adsorption performance was evaluated at different Na^+ concentrations. The results indicated that $(\text{NH}_4)_2\text{S}_2\text{O}_8$ -eluted LMO nanotubes remained 88.32% of Li^+ adsorption capacity when the ratio of $\text{Na}^+:\text{Li}^+$ was increased to 10:1 (Figure S7B).

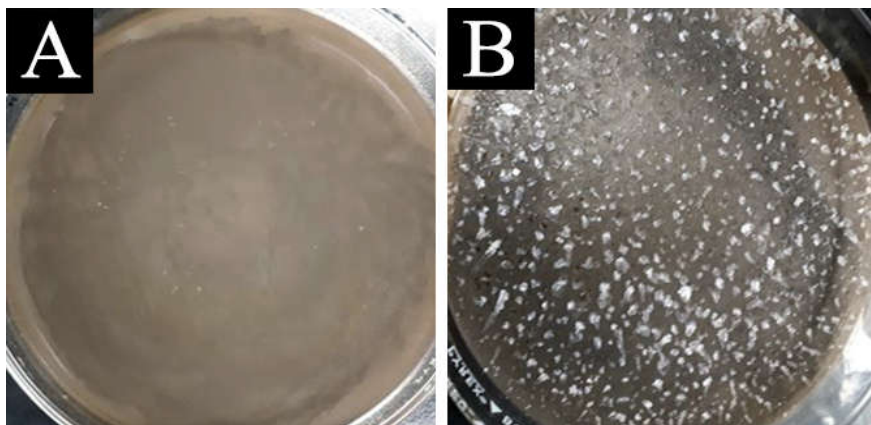


Figure S8 Nanotube adsorbents after recovery tests using A) 0.05 and B) 0.1 mol L⁻¹ Li⁺, Na⁺, K⁺, and Mg²⁺ brines. The tests were carried out at 60°C while stirring at 200 rpm for 1 h. The presence of white crystals indicated that the washing step is insufficient to remove salts, which is not adsorbed by the sorbent in simulated brine. Related to Figure 4 and Table 1.

Table S1 Comparison of the extraction strategy developed in this work with other studies. Related to Figure 4.

Materials	Synthesis method	Sample	Li ⁺ concentration (mg/L)	T/pH	Li ⁺ uptake (mg/g)	Q _{th} (mg/g)	Efficiency (%)	Manganese dissolution	Reference
Li _{1.33} Mn _{1.67} O ₄	solid-phase	Natural	1458	25°C/6.	30	56	54	1.30%	(Ohashi and Tai, 2019)
		Brine		5					
Li _{1.33} Mn _{1.67} O ₄ /Al ₂ O ₃	solid-phase	Natural	1458	25°C/6.	35	56	63	0.99%	(Ohashi and Tai, 2019)
		Brine		5					
Li _{1.33} Mn _{1.67} O ₄ /NiO	solid-phase	Natural	1458	25°C/6.	36	56	64	1.15%	(Ohashi and Tai, 2019)
		Brine		5					
Li ₄ Mn ₅ O ₁₂	solid-phase	Qarhan	179	25°C/6.	3	56	5	1.90%	(Xiao et al., 2015)
		Brine		4					
Li ₄ Mn ₅ O ₁₂	solid-phase	LiCl	69	30°C/1	40	56	71	1.90%	(Xiao et al., 2015)
		solution		0.1					
LiMn ₂ O ₄	hydrothermal	LiCl	69.4	30°C/1	21	38	55	N/A	(Zhang et al., 2010)
		solution		0.1					
Li _{1.6} Mn _{1.6} O ₄	solid-phase	LiCl	83	25°C/N	32	68	47	4.00%	(Qian et al., 2020)
		solution							
LiMn ₂ O ₄	Spray Pyrolysis	LiOH	20	25°C/N	35	38	90	N/A	(Özgür, 2010)
		solution							
LiMn ₂ O ₄	solid-phase	LiOH	20	25°C/N	33	38	85	N/A	(Özgür, 2010)
		solution							
LiMn ₂ O ₄	hydrothermal	LiCl·H ₂ O	50	18°C/1	25	38	64	3.90%	(Yang et al., 2018)
		solution		0.0					
Li _{1.33} Mn _{1.67} O ₄	solid-phase	Li-spiked	30	16°C/7	10	56	54	N/A	(Hong et al., 2013)
		Seawater		-8					
Li ₄ Mn ₅ O ₁₂ /CTS	solid-phase	geotherm	25.78	30°C/1	9	56	16	0.60%	(Wang et al., 2020)
		al water		2					
Li ₂ TiO ₃ /PVC	solid-phase	geotherm	25.78	55°C/1	12.84	127	10	N/A	(Lin et al., 2019)
		al water		2					
Li _{1.1} Mn _{1.9} O ₄	hydrothermal	LiCl	694	60°C/8.	39	44	90	0.08%	This work
		solution		0					

Q_{th} is the theoretical adsorption capacity of sorbent, calculated based on its composition; whereas the efficiency is obtained using a measured Li⁺ uptake divided by the theoretical adsorption capacity.

Reference

- Britto, S., and Kamath, P.V. (2014). Synthesis, structure refinement and chromate sorption characteristics of an Al-rich bayerite-based layered double hydroxide. *Journal of Solid State Chemistry* *215*, 206-210.
- Hong, H.-J., Park, I.-S., Ryu, T., Ryu, J., Kim, B.-G., and Chung, K.-S. (2013). Granulation of $\text{Li}_{1.33}\text{Mn}_{1.67}\text{O}_4$ (LMO) through the use of cross-linked chitosan for the effective recovery of Li^+ from seawater. *Chemical Engineering Journal* *234*, 16-22.
- Lin, H., Yu, X., Li, M., Duo, J., Guo, Y., and Deng, T. (2019). Synthesis of Polyporous Ion-Sieve and Its Application for Selective Recovery of Lithium from Geothermal Water. *ACS Appl Mater Interfaces* *11*, 26364-26372.
- Majzoub, E.H., and Rönnebro, E.C.E. (2012). Methodology of materials discovery in complex metal hydrides using experimental and computational tools. *Materials Science and Engineering: R: Reports* *73*, 15-26.
- Marthi, R., and Smith, Y.R. (2019). Selective recovery of lithium from the Great Salt Lake using lithium manganese oxide-diatomaceous earth composite. *Hydrometallurgy* *186*, 115-125.
- Ohashi, F., and Tai, Y. (2019). Lithium adsorption from natural brine using surface-modified manganese oxide adsorbents. *Mater Lett* *251*, 214-217.
- Özgür, C. (2010). Preparation and characterization of LiMn_2O_4 ion-sieve with high Li^+ adsorption rate by ultrasonic spray pyrolysis. *Solid State Ionics* *181*, 1425-1428.
- Qian, F., Zhao, B., Guo, M., Li, J., Liu, Z., and Wu, Z. (2020). K-gradient doping to stabilize the spinel structure of $\text{Li}_{1.6}\text{Mn}_{1.6}\text{O}_4$ for $\text{Li}^{(+)}$ recovery. *Dalton Trans* *49*, 10939-10948.
- Ryu, T., Haldorai, Y., Rengaraj, A., Shin, J., Hong, H.-J., Lee, G.-W., Han, Y.-K., Huh, Y.S., and Chung, K.-S. (2016). Recovery of Lithium Ions from Seawater Using a Continuous Flow Adsorption Column Packed with Granulated Chitosan–Lithium Manganese Oxide. *Industrial & Engineering Chemistry Research* *55*, 7218-7225.
- Wang, H., Cui, J., Li, M., Guo, Y., Deng, T., and Yu, X. (2020). Selective recovery of lithium from geothermal water by EGDE cross-linked spherical CTS/LMO. *Chemical Engineering Journal* *389*.
- Xiao, J., Nie, X., Sun, S., Song, X., Li, P., and Yu, J. (2015). Lithium ion adsorption–desorption properties on spinel $\text{Li}_4\text{Mn}_5\text{O}_{12}$ and pH-dependent ion-exchange model. *Advanced Powder Technology* *26*, 589-594.
- Yang, F., Chen, S., Shi, C., Xue, F., Zhang, X., Ju, S., and Xing, W. (2018). A Facile Synthesis of Hexagonal Spinel $\lambda\text{-MnO}_2$ Ion-Sieves for Highly Selective Li^+ Adsorption. *Processes* *6*.
- Zhang, Q.-H., Li, S.-P., Sun, S.-Y., Yin, X.-S., and Yu, J.-G. (2010). LiMn_2O_4 spinel direct synthesis and lithium ion selective adsorption. *Chemical Engineering Science* *65*, 169-173.